Spin-glass phases in stage-2 $FeCl_3$ graphite intercalation compound

Masatsugu Suzuki and Itsuko S. Suzuki
Department of Physics, State University of New York at Binghamton, Binghamton, New York 13902-6016
(Received 22 January 1998)

The magnetic phase transitions of stage-2 $FeCl_3$ graphite intercalation compound have been studied using superconducting quantum interference device dc and ac susceptibility measurements in the temperature range between 1.9 and 18 K. The temperature, frequency, and field dependence of χ'_{aa}, χ''_{aa}, χ'_{cc}, and χ''_{cc} clearly show that this compound undergoes two kinds of spin-glass phase transition at $T_{SG}^{(h)}$ ($\approx 4.5-6.1$ K) and $T_{SG}^{(l)}$ ($\approx 2-2.5$ K), respectively. Both χ''_{aa} and χ''_{cc} have peaks at $T_{SG}^{(h)}$ that shift to the low-temperature side with decreasing frequency. The spin-glass phase below $T_{SG}^{(h)}$ may result from a competition between the antiferromagnetic XY-like Fe^{3+} spins as the majority and the ferromagnetic Ising Fe^{2+} spins as the minority. The absorption χ''_{aa} has a peak at $T_{SG}^{(l)}$ that shifts to the low-temperature side with decreasing frequency. No anomaly in χ''_{cc} is observed at $T_{SG}^{(l)}$, indicating that only the XY components of spins contribute to this transition. The spin-glass transition below $T_{SG}^{(l)}$ may result from a competition between the intraplanar nearest-neighbor antiferromagnetic and next-nearest-neighbor ferromagnetic intraplanar exchange interaction, which is responsible for a possible incommensurate in-plane spin structure at low temperatures. [S0163-1829(98)01725-1]

I. INTRODUCTION

$FeCl_3$ graphite intercalation compounds (GIC's) provide a model system for studying the magnetic phase transition of a two-dimensional (2D) spin system. The magnetic properties of $FeCl_3$ GIC's have been studied by many researchers for almost three decades.[1–20] The pioneering work of the magnetic study on $FeCl_3$ GIC's was made by Karimov and co-workers.[1] They showed that the magnetic susceptibility of polycrystalline samples has a peak at 3.6 K for stage-1 GIC and at 7 K for stage-2 GIC, which is identified as the onset of antiferromagnetic and ferromagnetic phase transitions, respectively. Ohhashi and Tusjikawa[2,3] made the Mössbauer and dc magnetic susceptibility measurements of stage-1 and stage-2 $FeCl_3$ GIC based on highly oriented pyrolytic graphite (HOPG) and a single crystal of kish graphite (SCKG). They showed that both stage-1 and stage-2 compounds undergo antiferromagnetic phase transitions at the Néel temperature $T_N = 3.9$ K for stage 1 and 3.6 K for stage 2, where spins lie in the c plane perpendicular to the c axis. Holwein *et al.*[4] made the Mössbauer and dc magnetic susceptibility measurements of stage-1 $FeCl_3$ GIC. They showed that the Curie-Weiss temperature is $\Theta = -5$ K, indicating an antiferromagnetic exchange interaction. The temperature variation of the hyperfine field leads to $T_N = 4.1 \pm 0.2$ K. Millman and co-workers[5] measured the ac susceptibility of stage-1 and stage-2 $FeCl_3$ GIC's based on HOPG for orientations both parallel and perpendicular to the c axis. They showed that stage-1 and stage-2 compounds undergo a magnetic phase transition at 4.3 ± 0.2 K and 1.3 ± 0.2 K, respectively. Millman and Zimmerman[6] measured the ac magnetic susceptibility of stage-2 $FeCl_3$ GIC based on HOPG. They showed that the ac magnetic susceptibility has a sharp peak at 1.7 K. This peak is dramatically enhanced as the number of Fe^{3+} sites, which are nearest neighbors to iron vacancies, is increased from 7 to 11%. Ibrahim and Zimmerman[7,8] measured the ac magnetic susceptibility of stage-1 to stage-6 $FeCl_3$ GIC along the c plane and the c axis. They showed that the ac magnetic susceptibility along the c plane has a sharp peak at 1.7 and 1.8 K for all stages. The peak is dramatically reduced when a magnetic field of the order of 5 Oe along the c plane is applied. As the magnetic field increases, the peak shifts to the high-temperature side, indicating the occurrence of a ferromagnetic phase transition with 2D character. No peak is observed in the ac susceptibility along the c axis.

Miyoshi *et al.*[9] measured the temperature dependence of the ac magnetic susceptibility for stage-3 $FeCl_3$ GIC including the dispersion χ', absorption χ'', and nonlinear magnetic susceptibility χ_2. The dispersion χ' shows a peak at temperature T_h (≈ 5.2 K) for $f = 3.7$ Hz that shifts to the high-temperature side with increasing frequency f. The absorption χ'' rapidly increases near T_h and seems to have an inflection point at T_h. These behaviors in χ' and χ'' suggest an occurrence of a spin-glass phase at T_h. The nonlinear magnetic susceptibility χ_2 shows a sharp negative peak around T_h, suggesting further evidence of the spin-glass phase.

In spite of a considerable amount of work it seems that the magnetic phase transition of $FeCl_3$ GIC has not been sufficiently understood compared to that of the other transition metal dichloride GIC's such as $CoCl_2$ GIC and $NiCl_2$ GIC.[10,11] In particular, the relation between the phase transition at 1.7 K and that near 4 K remains unclear. In this paper we report an extensive study on the magnetic phase transitions of stage-2 $FeCl_3$ GIC using dc superconducting quantum interference device (SQUID) magnetization (zero-field-cooled magnetization and field-cooled magnetization) and ac SQUID magnetic susceptibility. Since the magnetic phase transition of stage-2 $FeCl_3$ GIC is expected to be very sensitive to the remanent magnetic field, all these measurements are made after the system is cooled from 300 to 1.9 K in the zero magnetic field (typically less than 3 mOe). The frequency, temperature, and magnetic-field dependence of the dispersion (χ'_{aa} and χ'_{cc}) and the absorption (χ''_{aa} and χ''_{cc})

along the c plane and the c axis, respectively, are examined in detail. The magnetic phase transitions of stage-2 $FeCl_3$ GIC are very complicated because of spin frustration effects arising from competing interactions and spin anisotropies. We will show that two kinds of spin-glass phase occur at temperatures $T_{SG}^{(h)}$ and $T_{SG}^{(l)}$.

In Sec. II we present a simple review of the experimental results on Mössbauer and magnetic neutron scattering of stage-1 and stage-2 $FeCl_3$ GIC's. In Secs. III and IV the experimental procedure and results are given. In Sec. V the results are discussed in the light of the spin-glass phase and compared with data reported previously.

II. MAGNETIC PROPERTIES OF $FeCl_3$ GIC'S

A. Mössbauer effect

The Mössbauer effect of $FeCl_3$ GIC's has been extensively studied by several groups.[2,4,12–16] Millman and Kirczenow[16] have shown that there are three kinds of Fe site in the $FeCl_3$ intercalate layers of stage-1 and stage-2 $FeCl_3$ GIC's. Their results for stage-2 $FeCl_3$ GIC are as follows. (i) The majority Fe^{3+} ions (site A) have the same isomer shift ($\delta=0.58$ mm/s) as pristine $FeCl_3$. It possesses a small quadrupole splitting $\Delta E_Q=0.23\pm0.03$ mm/s with symmetric peak intensities. The percent contribution of majority Fe^{3+} decreases from 86.6% at 90 K to 75.6% at 10 K. The major axis of the electric-field-gradient tensor lies along the c plane perpendicular to the c axis. The full six-line hyperfine pattern with the intensity ratio of 3:4:1:1:4:3 is observed at low temperatures for the γ ray parallel to the c axis, indicating that the easy axis of the majority Fe^{3+} spins lies in the c plane. (ii) The minority Fe^{2+} ions (site B) have an isomer shift $\delta=1.21$ mm/s and a quadrupole splitting $\Delta E_Q=-1.85$ mm/s. The percent contribution of Fe^{2+} ions increases from 4% at 90 K to 17% at 10 K as the temperature decreases. Note that the isomer shift of site B is the same as that for $FeCl_2$ GIC's. Ohhashi and Tsujikawa[17] have shown that there are two kinds of Fe^{2+} sites in stage-2 $FeCl_2$ GIC: $\delta=1.21$ mm/s and $\Delta E_Q=2.20$ mm/s, and $\delta=1.20$ mm/s, $\Delta E_Q=1.35$ mm/s. The major axis of the electric-field-gradient tensor lies along the c axis, suggesting that the Fe^{2+} spins are aligned along the c axis. (iii) The minority Fe^{3+} ions (site C) that are next neighbors to iron vacancies have $\delta=0.58$ mm/s and $\Delta E_Q=1.27$ mm/s. The percent contribution of Fe^{3+} ions with site C remains unchanged: 7.4% at 90 and 10 K. The number of iron vacancies is one third of the number of Fe^{3+} sites nearest neighbors to iron vacancies (2.8%). The full six-line hyperfine pattern with the intensity ratio of 3:2:1:1:2:3 is observed at 65 mK, when the γ-ray direction is parallel to the c axis. No change in δ was observed between 10 K and 65 mK, indicating no occurrence of a magnetically ordered phase.

Ohhashi and Tsujikawa[2] reported that the percent contribution of majority Fe^{2+} is less than 3%, which is rather different from that (17% at 10 K) derived by Millman and Kirczenow.[16] According to the comment by Millman and Kirczenow,[16] a careful reexamination of the spectra of Ohhashi and Tsujikawa[2] shows that there is a noticeable concentration of Fe^{2+} present in their sample in spite of their claim. Holwein *et al.*[4] have reported that the percent contribution of Fe^{2+} is 20% for stage-1 $FeCl_3$ GIC. The internal magnetic field H_n ($=500$ kOe at 0 K) from the hyperfine splitting dramatically decreases with increasing temperature and reduces to zero at T_N ($=4$ K) for stage-1 and stage-2 $FeCl_3$ GIC's. This result is a little different from that obtained by Millman and co-workers:[12] $H_n=452$ kOe at 0 K for stage 1 and stage 2, and $T_N=4.2\pm0.5$ K for stage 1 and 2.0 ± 1.5 K for stage-2 $FeCl_3$ GIC.

B. Magnetic neutron scattering

There have been few studies on the magnetic neutron scattering of $FeCl_3$ GIC's. Here we present a simple review on the magnetic neutron-scattering studies on stage-1 and stage-2 $FeCl_3$ GIC's that were done by Simon *et al.*[18–20] They have shown that there are two types of phase in samples of $FeCl_3$ GIC's: α phase and β phase. The β phase is usually found in powdered $FeCl_3$ GIC's, while the α phase exists in $FeCl_3$ GIC's based on HOPG and SCKG. The action of water in air on the α phase leads to the β phase. No difference in structure is observed between the α and β phases. The principal axis of the $FeCl_3$ lattice is rotated by 30° with respect to that of the graphite lattice. In the $FeCl_3$ intercalate layers the Fe atoms form a honeycomb lattice with a lattice constant $a_h=6.12$ Å in the octahedral sites of the chlorine lattice. The fundamental reciprocal lattice vectors are given by $\mathbf{a}^*$ and $\mathbf{b}^*$ with $|\mathbf{a}^*|=|\mathbf{b}^*|=4\pi/(\sqrt{3}a_h)=1.185$ Å^{-1}.

For stage-1 $FeCl_3$ GIC with β phase, the magnetic Bragg peaks appear at the in-plane wave vector $\mathbf{Q}=\mathbf{k}_1$, $\mathbf{k}_2$, $\mathbf{a}^*-\mathbf{k}_1$, $\mathbf{a}^*-\mathbf{k}_2$, and so on. Here $\mathbf{k}_1$ and $\mathbf{k}_2$ are the in-plane reciprocal lattice vectors for the incommensurate magnetic modulation: $|\mathbf{k}_1|=|\mathbf{k}_2|=0.394|\mathbf{a}^*|=0.467$ Å^{-1} and the angle between $\mathbf{k}_1$ and $\mathbf{k}_2$ is 60°. The angle between $\mathbf{k}_1$ and $\mathbf{a}^*$, θ, is determined from a relation

$$\cos\theta=\frac{|\mathbf{k}_1|^2+|\mathbf{a}^*|^2-|\mathbf{k}_1-\mathbf{a}^*|^2}{2|\mathbf{k}_1||\mathbf{a}^*|}. \tag{1}$$

When $|\mathbf{k}_1-\mathbf{a}^*|=0.72$ Å^{-1} the value of $\cos\theta$ is nearly equal to 1, suggesting that $\mathbf{k}_1$ is parallel to $\mathbf{a}^*$. The integrated magnetic scattering intensity at $\mathbf{Q}=\mathbf{k}_1$ decreases to zero at 3.8 K, indicating the occurrence of a magnetic phase transition. A strong 2D spin correlation develops below 30 K.

For stage-2 $FeCl_3$ GIC with β phase, the magnetic Bragg peak also appears at $\mathbf{Q}=\mathbf{k}_1$ with $|\mathbf{k}_1|/|\mathbf{a}^*|=0.394$. The magnetic peak is asymmetric and has a Warren shape characteristic of 2D spin correlations. The integrated magnetic scattering intensity increases gradually as the temperature decreases, showing no evidence for the magnetic phase transition. A strong 2D spin correlation develops below 30 K.

For stage-1 $FeCl_3$ GIC with α phase, the magnetic Bragg peak appears at the commensurate in-plane wave vector $\mathbf{Q}=\mathbf{k}_1$ with $|\mathbf{k}_1|=0.25|\mathbf{a}^*|\approx0.30$ Å^{-1} where the angle between $\mathbf{k}_1$ and $\mathbf{a}^*$ may be zero. Weakness of signal indicates that only a small part of the spins are ordered below 1.7 K where the ac susceptibility shows a peak.

III. EXPERIMENTAL PROCEDURE

Our samples were prepared by intercalating a single crystal of $FeCl_3$ into HOPG using the two-bulb method. The

temperatures of graphite and $FeCl_3$ were held at 300 °C and 380 °C, respectively. This condition is the same as those reported by Mizutani *et al.*[21] The reaction was made in a Pyrex glass tubing sealed in vacuum for two weeks. The stoichiometry of the sample was determined as $C_{13.77\pm0.01}FeCl_3$ from the weight uptake measurement when Fe ions are assumed to exist as $FeCl_3$ in the intercalate layer. The sample was confirmed from the (00L) x-ray diffraction to be well-defined stage 2 with the c axis repeat distance 12.78 ± 0.02 Å. The ideal stoichiometry is estimated as $C_{12.38}FeCl_3$ when Fe ions are ideally situated on the honeycomb lattice with the lattice constant $a_h = 6.12$ Å. The filling factor is estimated as 89.9% if the sample is formed of only stage 2.

The ac magnetic susceptibility and dc magnetization were measured using a SQUID magnetometer (Quantum Design, MPMS XL-5) with an ultralow-field capability option. (i) ac magnetic susceptibility measurement. The sample was cooled from 298 K to 1.9 K in a zero magnetic field (less than 3 mOe). Then the temperature (T) dependence of dispersion χ' and absorption χ'' was measured between 1.9 and 18 K in the absence and presence of H. The amplitude of the ac magnetic field h was 500 mOe and 25 different frequencies between 0.01 Hz and 1 kHz were chosen. (ii) dc magnetization measurement. The sample was cooled from 298 K to 1.9 K in a zero magnetic field (less than 3 mOe). Then an external magnetic field H ($=1$ Oe) was applied at 1.9 K. The zero-field-cooled magnetization ($M_{\rm ZFC}$) was measured with increasing temperature from 1.9 to 25 K and the field-cooled magnetization ($M_{\rm FC}$) was measured with decreasing temperature from 25 to 1.9 K. (iii) The dc magnetic susceptibility was also measured between 1.9 and 300 K in the presence of H ($1 \leqslant H \leqslant 50$ kOe).

IV. RESULTS

A. dc magnetization and magnetic susceptibility

Figure 1(a) shows the temperature (T) dependence of the dc magnetic susceptibility χ_a along the c plane and χ_c along the c axis in the presence of an external magnetic field of $H = 1$ kOe. The susceptibility χ_a is larger than χ_c in the temperature range between 1.9 and 300 K, showing an easy-plane-type spin anisotropy of this system. The susceptibility χ_a has a peak at 2.61 ± 0.02 K, while χ_c has no anomaly at any temperature. The susceptibility χ_a and χ_c obey the Curie-Weiss law at high temperatures. The least-squares fit of the data of χ_a vs T and χ_c vs T to the Curie-Weiss law for $150 \leqslant T \leqslant 300$ K yields the Curie-Weiss temperature Θ and Curie-Weiss constant C: $\Theta_a = -5.64 \pm 1.12$ K, $C_a = 5.22 \pm 0.06$ emu K/mol, and $\Theta_c = -10.94 \pm 0.98$ K, $C_c = 5.04 \pm 0.05$ emu K/mol. These values are in good agreement with those for stage-2 $FeCl_3$ GIC reported by Ohhashi and Tsujikawa:[3] $\Theta_a = -6.0 \pm 1.0$ K, $C_a = 4.46 \pm 0.10$ emu K/mol, $\Theta_c = -9.0 \pm 2.0$ K, and $C_c = 4.30 \pm 0.05$ emu K/mol. Figure 1(b) shows the T dependence of reciprocal susceptibility $(\chi_i - \chi_i^0)^{-1}$ for $i = a$ and c, where χ_i^0 is a temperature-independent susceptibility determined from the least-squares fit.

The inset of Fig. 1(a) shows the field (H) dependence of the magnetization M_a at 1.9 K in the presence of H along the

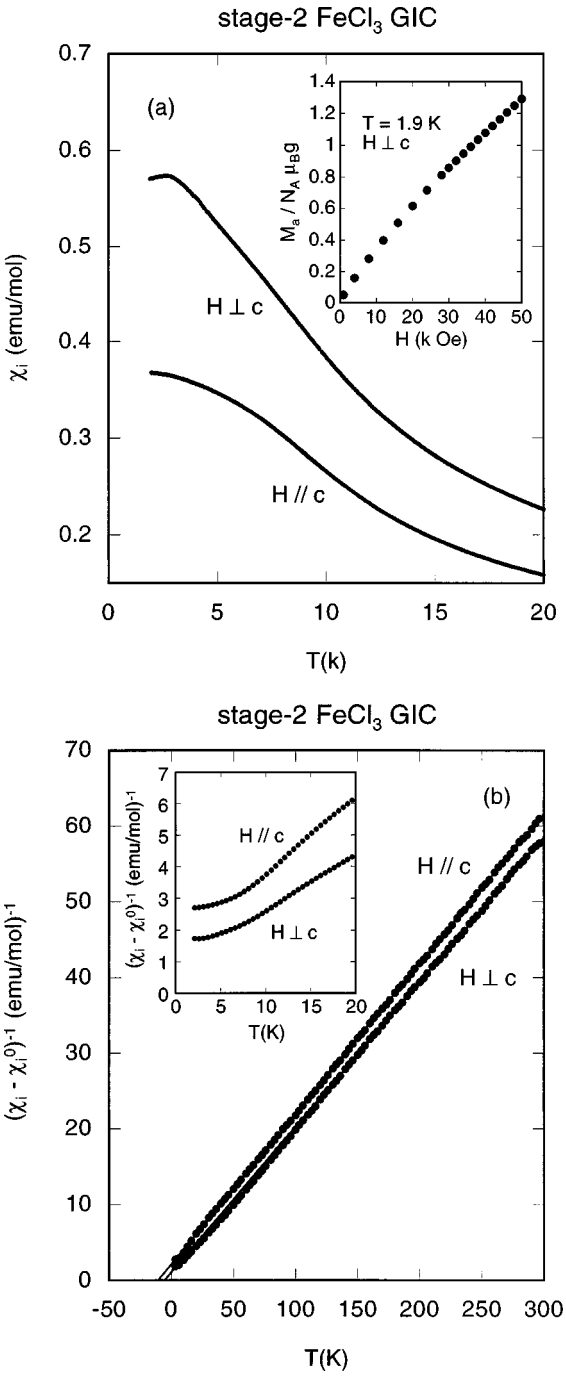

FIG. 1. (a) T dependence of χ_a ($H \perp c$) and χ_c ($H \| c$) at $H = 1$ kOe for stage-2 $FeCl_3$ GIC. The inset shows the H dependence of normalized magnetization $M_a/N_A g\mu_B (= \langle S \rangle)$ at 1.9 K for $H \perp c$ with $g = 2$ and $N_A\mu_B = 5.585 \times 10^3$ emu. (b) T dependence of reciprocal susceptibilities $(\chi_i - \chi_i^0)^{-1}$ at $H = 1$ kOe for $i = a$ and c.

c plane. The normalized magnetization defined by $M_a/gN_A\mu_B$ corresponds to the average spin $\langle S \rangle$, where $gN_A\mu_B = 1.117 \times 10^4$ emu/mol with $g = 2$. (i) $\langle S \rangle = 0$ for $H \approx 0$, suggesting the antiferromagnetic intraplanar exchange interaction. (ii) the slope defined by $d\langle S \rangle/dH$ changes around $H = 30$ kOe where $\langle S \rangle \approx S/3$ with $S = \frac{5}{2}$, suggesting that the spin-flop field $H_{\rm SF}$ is of the order of 30 kOe.

In Fig. 2 we show the T dependence of zero-field-cooled magnetization $M_{\rm ZFC}$ and field-cooled magnetization $M_{\rm FC}$ in the presence of H ($=1$ Oe) along the c plane and the c axis,

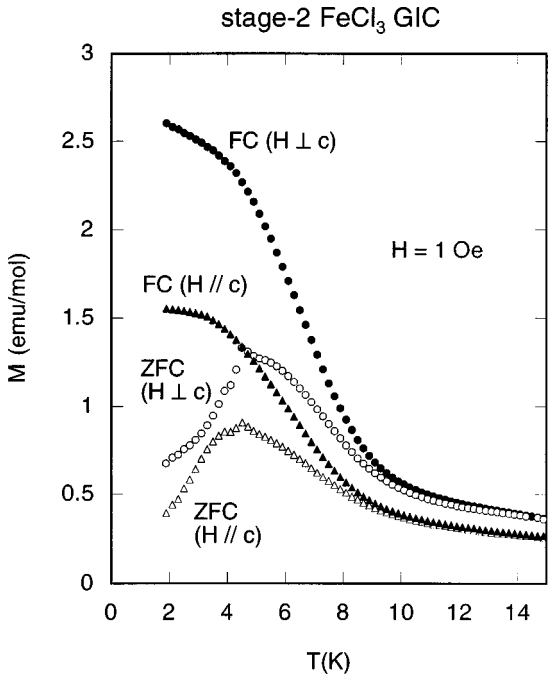

FIG. 2. T dependence of zero-field-cooled magnetization M_{ZFC} and field-cooled magnetization M_{FC} for $H\perp c$ and $H\|c$. $H=1$ Oe.

respectively. Both M^a_{ZFC} and M^c_{ZFC} have broad peaks at 4.5 K. Note that a discontinuity in M_{ZFC} observed around 4 K may be due to an uncertainty of temperature occurring during the measurements. The deviation of M_{FC} from M_{ZFC} appears at 14.7 K for the c plane and 24 K for the c axis, indicating the occurrence of an irreversible effect of magnetization. Both M^a_{FC} and M^c_{FC} tend to saturate below 4 K and 3.1 K, respectively. The value of M^a_{FC} is larger than that of M^c_{FC} at least for $1.9\leqslant T\leqslant 25$ K, indicating the XY spin anisotropy of this system.

B. ac magnetic susceptibility χ'_{aa} and χ''_{aa} for $H=0$

Figure 3(a) shows the T dependence of the dispersion χ'_{aa} for typical frequencies. The dispersion χ'_{aa} exhibits a small shoulder at low temperature T_l and a broad peak at high temperature T_h. A broad peak at T_h shifts to the high-temperature side with increasing frequency: 5.26 K for $f=0.01$ Hz to 6.72 K for $f=1$ kHz. A shoulder at T_l also shifts to the high-temperature side: $T_l\approx 2.3$ K for 0.01 Hz to ≈ 3 K for 1 kHz. The peak height at T_h is strongly dependent on frequency: it decreases with increasing ω as $\chi'^{\,\max}_{aa}\approx\omega^{-0.0367\pm 0.0005}$.

Figure 3(b) shows the T dependence of absorption χ''_{aa} for typical frequencies. The absorption χ''_{aa} exhibits a small peak at low-temperature T_l and a broad peak at high-temperature T_h. A broad peak at T_h shifts to the high-temperature side with increasing frequency: 4.52 K at 0.01 Hz to 6.07 K for 1 kHz. The peak height of the broad peak at T_h is dependent on frequency: it decreases with increasing ω as $\chi''^{\,\max}_{aa}\approx\omega^{-0.0162\pm 0.0010}$. Figure 3(c) shows the T dependence of χ''_{aa} around T_l. The small peak at T_l shifts to the high-temperature side with increasing frequency: 1.95 K at 0.01 Hz to 2.52 K at 1 kHz [see also Fig. 3(d) shown later]. This result suggests that the transition is similar to one from the paramagnetic (PM) phase to the spin glass (SG) phase. The f dependence of this peak height is rather different from that at T_h. The peak height at T_l slightly decreases with increasing f for $0.01\leqslant f\leqslant 10$ Hz. It has a local minimum at 20 Hz, and rapidly increases with increasing frequency. Figure 3(d) shows the f dependence of the peak temperatures T_h for χ'_{aa}, χ''_{aa}, χ'_{cc}, and χ''_{cc} and T_l for χ''_{aa}. Note that the T dependence of χ'_{cc} and χ''_{cc} will be discussed below. The peak temperature T_h of χ'_{aa} is higher than the peak temperature T_h of χ''_{aa} by 0.65–0.74 K at the same frequency. The frequency dependence of T_h for χ''_{aa} will be discussed in more detail in Sec. V.

C. ac magnetic susceptibility χ'_{aa} and χ''_{aa} for H along the c plane

The T dependence of χ'_{aa} and χ''_{aa} with $f=1$, 10, and 100 Hz was measured in the presence of H along the c plane. In Fig. 4(a) we show the T dependence of χ'_{aa} with $f=1$ Hz for various magnetic fields. The broad peak at T_h shifts to the low-temperature side with increasing H: 6.35 K at $H=0$ and 3.85 K at 2 kOe. This may indicate that the low-temperature phase is an antiferromagnetic one with spins lying in the c plane. It seems that the shoulder at T_l remains unchanged at low fields but disappears above 200 Oe. In Fig. 4(b) we show the T dependence of χ''_{aa} with $f=1$ Hz for various magnetic fields. It clearly shows a broad peak at $T_h=5.03$ K and a small peak at $T_l=2.14$ K at $H=0$ Oe. The broad peak at T_h shifts to the low-temperature side with increasing H ($T_h=3.1$ K at $H=500$ Oe) and disappears above 700 Oe. The small peak at T_l slightly shifts to the low-temperature side as H increases ($T_l=2.07$ K at $H=200$ Oe) and disappears above 500 Oe. Figure 4(c) shows the H dependence of the peak temperature T_h for χ'_{aa} and χ''_{aa} with $f=1$, 10, and 100 Hz. The peak temperature T_h for χ'_{aa} and χ''_{aa} is related to magnitude of H through a power-law form described by

$$T_h(H)=T_h(H=0)\left[1-\left(\frac{H}{H_0}\right)^{1/\alpha}\right], \tag{2}$$

where α is an exponent. The least-squares fit of the data of T_h vs H for χ'_{aa} and χ''_{aa} in the limited field ranges yields the values of $T_h(H=0)$, H_0 and α for $f=1$, 10, and 100 Hz that are listed in Table I. This exponent α that is dependent on frequency and the kind of susceptibility is a little smaller than that ($\alpha=1.50$) predicted by Almeida and Thouless[22] for the field dependence of freezing temperature at the transition between the PM and SG phases. In contrast, the peak temperature T_l for χ''_{aa} remains almost unchanged with increasing H for $0\leqslant H\leqslant 100$ Oe: $T_l=2.14$–2.07 for $f=1$ Hz, $T_l=2.27$–2.21 K for $f=10$ Hz, and $T_l=2.38$–2.44 K for $f=100$ Hz.

The peak height $\chi'^{\,\max}_{aa}$ at T_h is dependent on the magnitude of H. The H dependence of $\chi'^{\,\max}_{aa}$ is described by a power law form in the field range between 20 and 200 Oe: $\chi'^{\,\max}_{aa}\approx H^{-\lambda}$ with the exponent $\lambda=0.485\pm 0.037$ for $f=1$ Hz, 0.444 ± 0.040 for $f=10$ Hz, and 0.423 ± 0.045 for $f=100$ Hz.

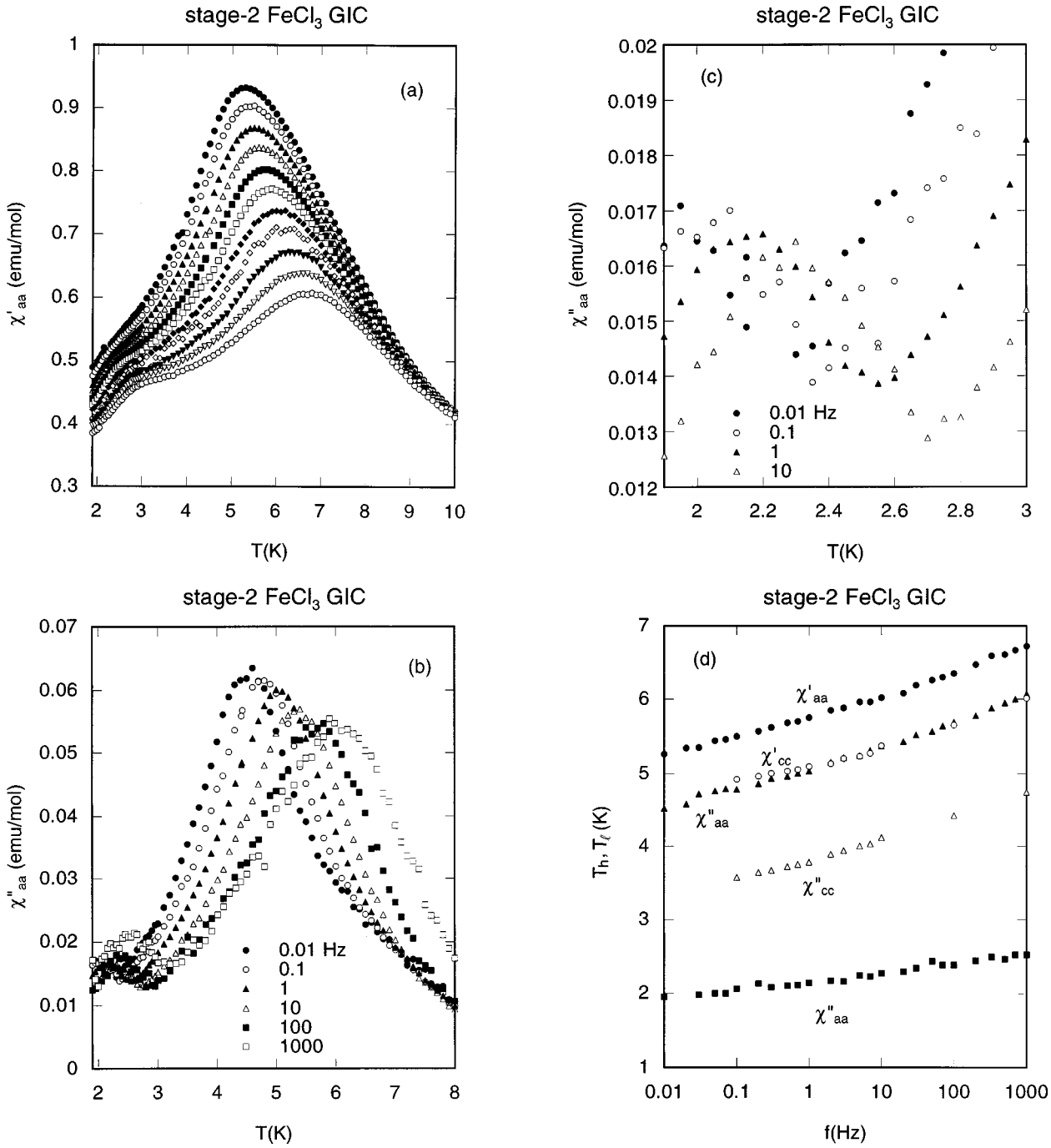

FIG. 3. (a) T dependence of dispersion χ'_{aa} at various frequencies: 0.01 (●), 0.03 (○), 0.1 (▲), 0.3 (△), 1 (■), 3 (□), 10 (♦), 30 (◇), 100 (▼), 330 (▽), and 1000 Hz (⊙). $h \perp c$. $h = 500$ mOe. $H = 0$. (b) T dependence of absorption χ''_{aa} at various frequencies. (c) T dependence of χ''_{aa} at various frequencies below 3 K. (d) f dependence of peak temperatures T_h and T_l for χ'_{aa} (●), χ''_{aa} (▲, ■) χ'_{cc} (○), and χ''_{cc} (△).

D. ac magnetic susceptibility χ'_{cc} and χ''_{cc} without H

Here we notice that a sample holder used only for the measurement of χ'_{cc} and χ''_{cc} gives rise to an appreciable frequency-dependent baseline to the ac susceptibility for $f > 100$ Hz partly because of the small values of χ'_{cc} and χ''_{cc}. Therefore, any data of χ'_{cc} and χ''_{cc} for $f \geqslant 200$ Hz are not used for discussing the magnitude of χ'_{cc} and χ''_{cc}. Figure 5(a) shows the T dependence of χ'_{cc} for $f \leqslant 100$ Hz in the absence of H. The dispersion χ'_{cc} has a broad peak at T_h, which shifts to the high-temperature side with increasing frequency: $T_h = 4.92$ K at 0.1 Hz to 6.01 K at 1 kHz. The peak temperature T_h of χ'_{cc} is almost the same as that of χ''_{aa} at the same frequency [see Fig. 3(d)]. The peak height decreases with increasing frequency as $\chi'_{cc} \approx \omega^{-0.0270 \pm 0.0004}$ for $0.1 \leqslant f \leqslant 100$ Hz. No anomaly in χ'_{cc} is observed near 2–3 K. This is in contrast to the shoulder observed in χ'_{aa} near 2–3 K. This result may suggest that only the XY spin components contribute to the spin ordering process at T_l. Figure 5(b) shows the T dependence of χ''_{cc} for $0.1 \leqslant f \leqslant 1$ Hz. The absorption χ''_{cc} has a relatively sharp peak at T_h, which shifts to the high-temperature side with increasing frequency: $T_h = 3.57$ Hz at 0.1 Hz to 4.74 K at 1 kHz. The peak tempera-

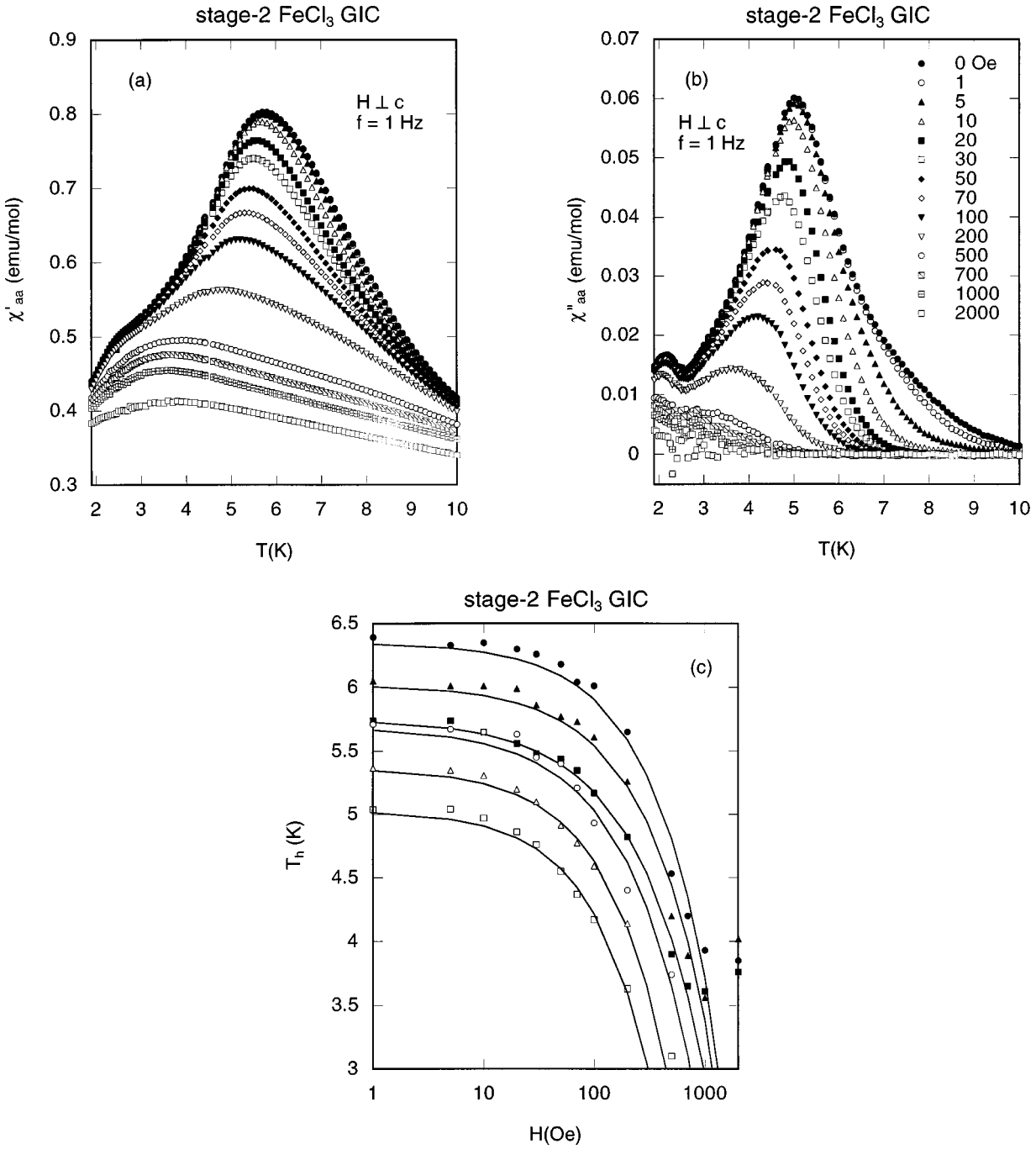

FIG. 4. T dependence of (a) χ'_{aa} and (b) χ''_{aa} for various magnetic fields H ($H\perp c$). $f=1$ Hz and $h=500$ mOe ($h\perp c$). The denotation for each field in (a) is the same as that in (b). (c) H dependence of peak temperature T_h for χ'_{aa} (●, ▲, ■), and χ''_{aa} (○, △, □) for $f=1$, 10, and 100 Hz, respectively. The solid lines are the least-squares fits of data to Eq. (2) with parameters listed in Table I.

ture T_h of χ''_{cc} is lower than that of χ'_{cc} by 1.27–1.35 K at the same frequency. Also, no anomaly in χ''_{cc} is observed around T_l.

E. ac magnetic susceptibility χ'_{cc} and χ''_{cc} with H along the c axis

Figures 6(a) and 6(b) show the T-dependence of χ'_{cc} and χ''_{cc} with $f=100$ Hz in the presence of various magnetic fields along the c axis. Figure 6(c) shows the H dependence of the peak temperature T_h for χ'_{cc} and χ''_{cc}. The peak temperature T_h of χ'_{cc} does not change with H for $H\leqslant 200$ Oe,

TABLE I. The exponent α for the field dependence of the peak temperature T_h for χ'_{aa} and χ''_{aa} defined by Eq. (2).

f (Hz)	T_h ($H=0$)	H_0 (kOe)	α	Field range of fitting
1 (χ'_{aa})	5.75 K	2.86	1.455±0.009	0–700 Oe
10 (χ'_{aa})	6.02 K	3.04	1.346±0.104	0–1 kOe
100 (χ'_{aa})	6.35 K	3.13	1.297±0.121	0–1 kOe
1 (χ''_{aa})	5.03 K	0.93	1.227±0.065	0–200 Oe
10 (χ''_{aa})	5.37 K	1.32	1.30±0.078	0–200 Oe
100 (χ''_{aa})	5.69 K	2.15	1.423±0.142	0–500 Oe

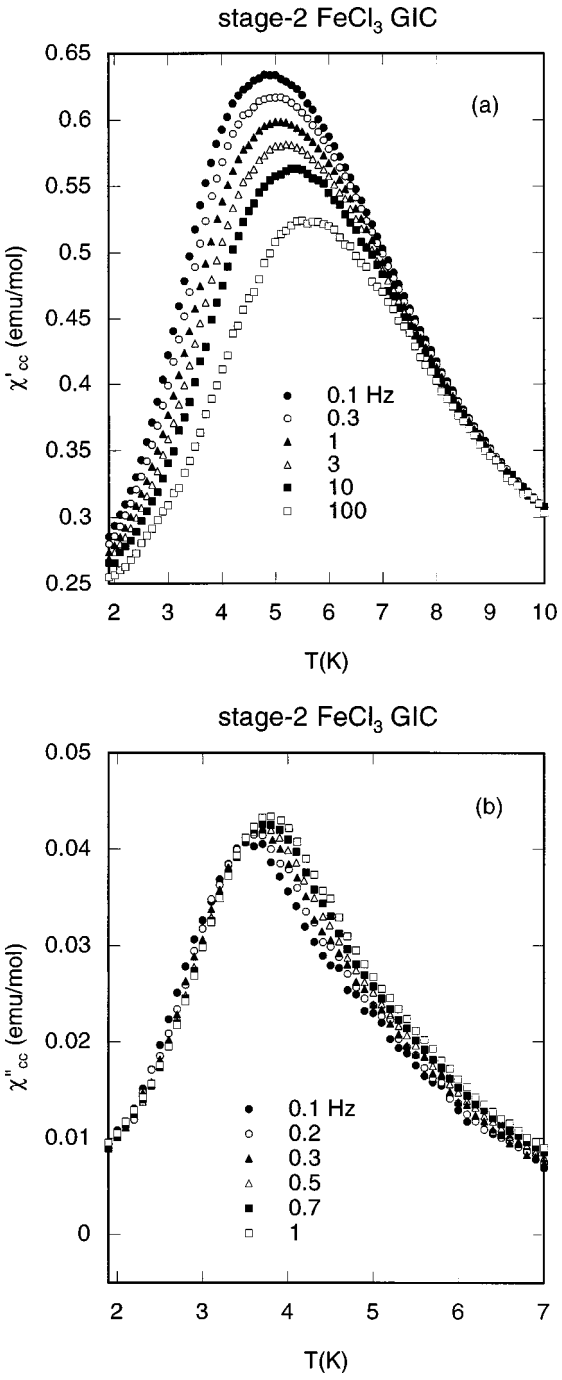

FIG. 5. T dependence of (a) χ'_{cc} and (b) χ''_{cc} for various frequencies. $H=0$. $h=500$ mOe. $h\|c$.

while the peak temperature T_h of χ''_{cc} decreases with H. The peak heights $\chi'^{\max}_{cc}$ and $\chi''^{\max}_{cc}$ at T_h are weakly dependent on the magnitude of H. The H dependence of $\chi'^{\max}_{cc}$ is described by a power-law form ($\chi'^{\max}_{cc} \approx H^{-\lambda}$) in the limited field range: $\lambda=0.182\pm0.008$ in χ'_{cc} for 50 Oe$\leqslant H \leqslant$2 kOe, 0.059 ± 0.003 in $\chi''^{\max}_{cc}$ for $30\leqslant H\leqslant 500$ Oe.

V. DISCUSSION

A. Spin Hamiltonian

The spin Hamiltonian of stage-2 $FeCl_3$ GIC may be described by

$$H=-2J\sum_{\langle i,j\rangle}\mathbf{S}_i\cdot\mathbf{S}_j+D\sum_i (S_i^z)^2, \tag{3}$$

with $S=\frac{5}{2}$ where J is the intraplanar exchange interaction and D is a single-ion anisotropy. According to Yosida,[23] the high-temperature susceptibility χ_a and χ_c along the c plane and along the c axis are given by

$$\chi_a=\frac{C}{T}\frac{1}{1-\Theta/T}\left(1+\frac{p}{T}\right)\approx\frac{C}{T-\Theta-p}, \tag{4}$$

$$\chi_c=\frac{C}{T}\frac{C}{1-\Theta/T}\left(1-\frac{2p}{T}\right)\approx\frac{C}{T-\Theta+2p}, \tag{5}$$

respectively, where C ($=N_A\mu_B^2P_{\rm eff}^2/3k_B$) is the Curie-Weiss constant and Θ [$=2zJS(S+1)/3$] is the Curie-Weiss temperature. The value of z is the number of nearest-neighbor Fe^{3+} ions and $z=3$. The parameter p is expressed by $p=D[2S(S+1)/15-1/10]$. The average susceptibility $\chi_{\rm av}$ [$=(\chi_c+2\chi_a)/3$] is derived from Eqs. (4) and (5) as a Curie-Weiss law $\chi=C/(T-\Theta)$. The least-squares fit of the data of χ vs T to this Curie-Weiss law yields $\Theta=-7.28\pm0.83$ K and $C=5.16\pm0.04$ (emu K/mol) in the temperature range between 150 and 300 K. The values of J and the effective magnetic moment $P_{\rm eff}$ are estimated as $J=-0.415\pm0.047$ K and $P_{\rm eff}=6.42\pm0.03\mu_B$, respectively. A negative sign of J indicates that the intraplanar exchange interaction is antiferromagnetic. The value of $P_{\rm eff}$ is a little larger than the spin-only-dependent value $g[S(S+1)]=5.91$ for $g=2$. The difference of two susceptibilities χ_d ($=\chi_a-\chi_c$) is calculated as $\chi_d=\chi_{\rm av}$ $(3p/T)$. The least-squares fit of the data $(\chi_d/\chi_{\rm av})$ vs T yields the value of p ($=0.782\pm0.093$) in the temperature range between 150 and 300 K. Note that the values of Θ and p can be also estimated using the relations $\Theta=(2\Theta_a+\Theta_c)/3$ and $p=(\Theta_a-\Theta_c)/3$: $\Theta=-7.41\pm1.07$ K and $p=1.77\pm0.70$ K for our result ($\Theta_a=-5.64\pm1.12$ K and $\Theta_c=-10.94\pm0.98$ K) and $\Theta=-7.0\pm1.3$ K and $p=1.0\pm1.0$ K for the results of Ohhashi and Tsujikawa ($\Theta_a=-6.0\pm1.0$ K and $\Theta_c=-9.0\pm2.0$ K).[3] The uncertainty of p thus obtained is much larger than that obtained by the first method.

Since $D=15p/16$ with $p=0.782\pm0.093$ K, the value of D is estimated as $D=0.733\pm0.087$ K. The positive sign of D is indicative of the easy-plane spin anisotropy of this system: spins lie in the c plane. Our value of D for stage-2 $FeCl_3$ GIC is close to that ($=0.58$ K) for the pristine $FeCl_3$ determined by Stamfel *et al.*[24] from Mössbauer measurements.

Once the values of J and D are determined, the intraplanar exchange field H_E $(2z|J|S/g\mu_B)$, the anisotropy field $H_A^{\rm out}$ $(=DS/g\mu_B)$, and the spin-flop (SF) field $[\approx(2H_EH_a^{\rm out})^{1/2}]$ can be estimated as $H_E=46.3\pm5.3$ kOe, $H_A^{\rm out}=13.6\pm1.6$ kOe, and $H_{\rm SP}=35.5$ kOe, respectively. This value of $H_{\rm SF}$ is comparable to that of the field ($H=30$ kOe) at which dM_a/dH at 1.9 K slightly changes as shown in the inset of Fig. 1(a). The susceptibility χ_c is expressed by $\chi_c=N_Ag^2\mu_B^2/4z|J|=3/(8z|J|)$. For $z=3$ and $|J|=0.415$ K, the value of χ_c is estimated as $\chi_c=0.30$ emu/mol, which is in good agreement with the value of χ_c ($=0.368$ emu/mol) at 1.9 K.

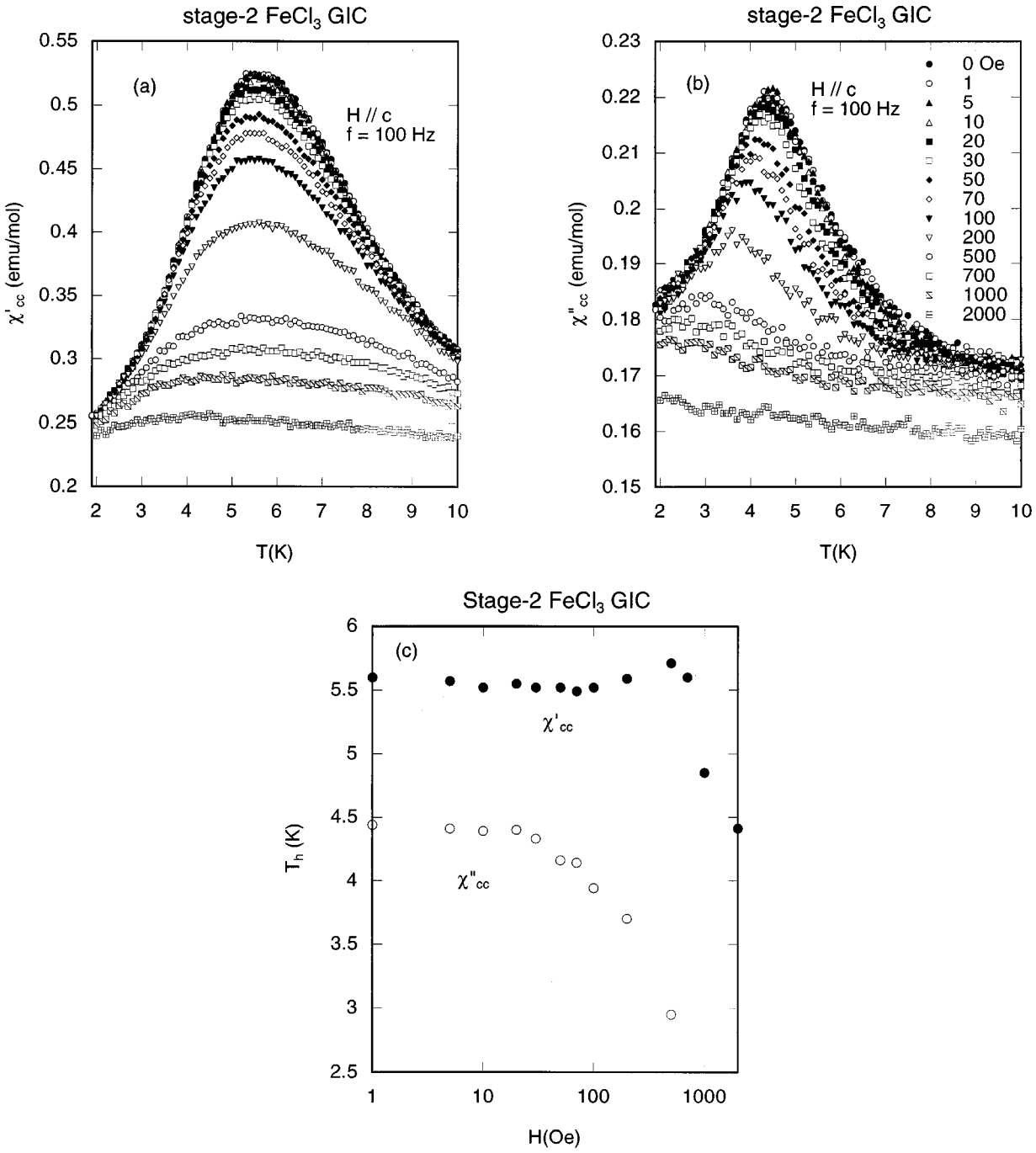

FIG. 6. T dependence of (a) χ'_{cc} and (b) χ''_{cc} for various magnetic fields ($H\|c$). $f=100$ Hz and $h=500$ mOe ($h\|c$). The denotation for each field in (a) is the same as that in (b). (c) H dependence of peak temperature T_h for χ'_{cc} and χ''_{cc} with $f=100$ Hz.

B. Estimate of next-nearest-neighbor exchange interactions

According to Simon *et al.*[18–20] stage-1 $FeCl_3$ GIC has a rather complicated in-plane spin structure characterized by the parameter $\delta\,(=|\mathbf{k}_1|/|\mathbf{a}^*|)$: $\delta=0.25$ for α phase and $\delta=0.394$ for β phase. As far as we know, there has been no work on the magnetic neutron scattering of stage-2 $FeCl_3$ GIC with α phase to which our system based on HOPG may belong. Here it may be reasonable to assume that the in-plane spin structure of stage-2 $FeCl_3$ GIC with α phase is the same as that of stage-1 $FeCl_3$ with α phase as is the case for the in-plane spin structure of β phase that exists in both stage-1 and stage-2 $FeCl_3$ GIC's. It is evident that these in-plane spin structures cannot be explained by the spin Hamiltonian given by Eq. (3) having only a nearest-neighbor (NN) intraplanar exchange interaction. The next-nearest-neighbor (NNN) intraplanar exchange interaction should be taken into account for the explanation of in-plane spin structures. The spin Hamiltonian of this system is assumed to consist of the intraplanar exchange interaction

$$H=-2\sum_{\langle i,j\rangle} J(\mathbf{R}_{ij})\mathbf{S}_i\cdot\mathbf{S}_j\,, \tag{6}$$

where $\mathbf{S}_i$ is the classical XY spin vector of an Fe^{3+} ion at the site $\mathbf{R}_i$ on the regular honeycomb lattice, and $\mathbf{R}_{ij}=\mathbf{R}_i-\mathbf{R}_j$. The parameter $J(\mathbf{R}_{ij})$ is the exchange interaction between

the spin $\mathbf{S}_i$ at the site $\mathbf{R}_i$ and the spin $\mathbf{S}_j$ at the site $\mathbf{R}_j$, where $J(-\mathbf{R}_{ij})=J(\mathbf{R}_{ij})$. The parameters J_0 and J_1 are the NN and the NNN intraplanar exchange interactions. Note that the anisotropic exchange interaction and the interplanar exchange interactions are not included in Eq. (6). The ground-state energy U_G of this system is described by

$$U_G=-NS^2J(\mathbf{Q}), \tag{7}$$

where $J(\mathbf{Q})$ is the sum of the Fourier components of the intraplanar exchange interaction

$$J(\mathbf{Q})=\sum_j J(\mathbf{R}_{ij})\exp(i\mathbf{Q}\cdot\mathbf{R}_{ij}), \tag{8}$$

and N is the total number of spins. The interaction $\mathbf{J}(\mathbf{Q})$ is assumed to have a maximum at the wave vector given by $\mathbf{Q}=(Q_1\mathbf{a}^*+Q_2\mathbf{b}^*)/2\pi$ and $\mathbf{a}^*$ and $\mathbf{b}^*$ are the reciprocal lattice vectors of the in-plane lattice structure. The angle between $\mathbf{a}^*$ and $\mathbf{b}^*$ is 120°. There are two Fe^{3+} ions per unit cell with $|\mathbf{a}|=|\mathbf{b}|=6.12$ Å, where the angle between $\mathbf{a}$ and $\mathbf{b}$ is 60°. There are three nearest-neighbor Fe^{3+} ions for each Fe^{3+} ions. Taking into account two Fe^{3+} sites in the unit cell, $J_0(\mathbf{Q})$ for the NN interactions and $J_1(\mathbf{Q})$ for the NNN interactions can be expressed as

$$J_0(\mathbf{Q})=2J_0\{\cos[(Q_1+Q_2)/3]+\cos[(-2Q_1+Q_2)/3]+\cos[(Q_1-2Q_2)/3]\} \tag{9}$$

and

$$J_1(\mathbf{Q})=4J_1[\cos(Q_1)+\cos(Q_2)+\cos(Q_1-Q_2)], \tag{10}$$

respectively. For fixed values of J_0 and J_1 the values of Q_1 and Q_2 for the stable in-plane spin structure can be determined from the following two conditions:

$$\frac{\partial J(\mathbf{Q})}{\partial Q_i}=0 \quad \text{and} \quad \frac{\partial^2 J(\mathbf{Q})}{\partial Q_i\partial Q_j}<0, \tag{11}$$

with $i,j=1,2$, where $J(\mathbf{Q})=J_0(\mathbf{Q})+J_1(\mathbf{Q})$. Note that the Curie-Weiss temperature Θ is described by

$$\Theta=\frac{2}{3}S(S+1)\left(\frac{J(\mathbf{Q}=0)}{2}\right)=\frac{2}{3}S(S+1)(3J_0+6J_1). \tag{12}$$

For the α phase the magnetic Bragg peak appears at $|\mathbf{Q}|=0.25\,|\mathbf{a}^*|$, where the exact position of $\mathbf{Q}$ in the reciprocal lattice plane has not been reported. For simplicity we consider the two cases (i) $Q_1/2\pi=0.25$ and $Q_2=0$ for the rotation angle $\theta=0°$ between $\mathbf{Q}$ and $\mathbf{a}^*$, and (ii) $Q_1/2\pi=-Q_2/2\pi=0.25/\sqrt{3}$ for $\theta=30°$. Then the above conditions (11) and (12) with $\Theta=-7.28\pm0.83$ K lead to antiferromagnetic J_0 and ferromagnetic J_1 for both cases: $J_0=-0.763\pm0.087$ K and $J_1=0.174\pm0.020$ K for case (i) and $J_0=-0.753\pm0.086$ K and $J_1=0.169\pm0.019$ K for case (ii). The values of J_0 and J_1 are almost independent of the rotation angle θ. The magnitude $|J_1|$ is not negligibly small compared to J_0. The competition between antiferromagnetic J_0 and ferromagnetic exchange interactions J_1 gives rise to a spin frustration effect.

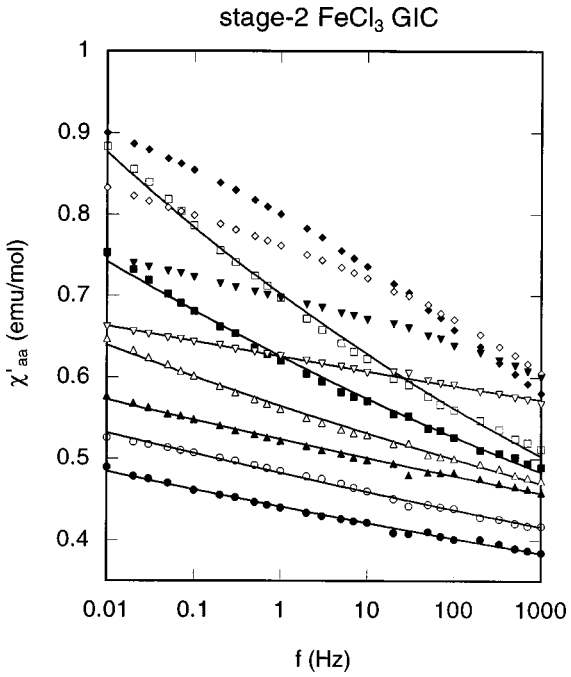

FIG. 7. f dependence of χ'_{aa} at various temperatures. $h=500$ mOe. $H=0$. $T=1.9$ (●), 2.3 (○), 2.9 (▲), 3.5 (△), 4.1 (■), 4.7 (□), 5.9 (◆), 6.5 (◇), 7.1 (▼), and 7.7 K (▽). The solid lines are the least-squares fits of data to the power-law form ($\chi'_{aa}\approx\omega^{-x}$).

On the other hand, for the β phase the magnetic Bragg peak appears at $\mathbf{Q}=\pm0.394\,\mathbf{a}^*,\pm0.394\,\mathbf{b}^*,\pm0.394(\mathbf{a}^*+\mathbf{b}^*)$, which corresponds to the case of $Q_1=0.394$ and $Q_2=0$. The conditions (11) and (12) lead to the values of J_0 and J_1, which seem to be unphysical: $J_0=-13.522\pm0.717$ K and $J_1=2.950\pm0.335$ K. This implies that the incommensurate spin structure cannot be explained by the above model: the higher-order interactions or interplanar interactions may not be neglected.

C. Nature of spin-glass phases at $T_{SG}^{(h)}$ and $T_{SG}^{(l)}$

Here we show that two different kinds of spin-glass phase occur at $T_h=T_{SG}^{(h)}$ (=4.3–6.1 K) and $T_l=T_{SG}^{(l)}$ (=2–2.5 K). Figure 7 shows the f dependence of χ'_{aa} at various T for $0.01\leqslant f\leqslant1000$ Hz. The dispersion χ'_{aa} decreases with increasing f at least in the temperature range $1.9\leqslant T\leqslant9.6$ K. The f dependence of χ'_{aa} is described by a power-law form ($\chi'_{aa}\approx\omega^{-x}$) over the whole frequency range except for $5.8\leqslant T\leqslant7.2$ K. The least-squares fit of the data to this power-law form yields the exponent x for each T. Figure 8 shows the T dependence of x thus obtained: it has a small peak ($x\approx0.023$) at 2.15 K and a large peak ($x\approx0.05$) at 5.0 K. Note that the T dependence of x is very similar to that of χ''_{aa} at $f=1$ Hz having a small peak at 2.14 K and a broad peak at 5.0 K.

Figures 9(a)–9(b) show the f dependence of χ''_{aa} at various T for $0.01\leqslant f\leqslant1000$ Hz. The f dependence of χ''_{aa} is rather different from that of χ'_{aa}. For $1.9\leqslant T\leqslant2.3$ K, χ''_{aa} seems to have a peak at f_l in the low-frequency region in spite of the noisy signals. This peak shifts to the high-frequency side with increasing temperature. The relation of T

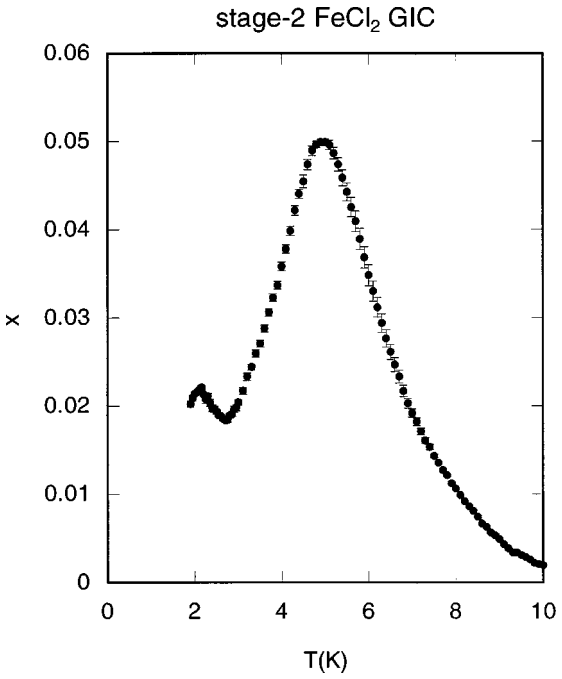

FIG. 8. T dependence of exponents x, where $\chi'_{aa} \approx \omega^{-x}$.

vs f_l thus obtained is equivalent to that of T_l vs f [see Fig. 3(d)] derived from the data of χ''_{aa} vs T with frequency as a parameter: T_l clearly increases with increasing frequency. Such behavior is common to spin-glass phases. The peak temperature T_l may correspond to the spin-glass freezing temperature $T_{\mathrm{SG}}^{(l)}$. The inset of Fig. 10 shows the average relaxation time τ_l as a function of temperature, where τ_l is determined using the relation that the peak of χ''_{aa} vs T appears when $\omega\tau_l = 1$ is satisfied. The average relaxation time τ_l divergingly increases with decreasing T. The most likely source for such a dramatic divergence of τ_l is a critical slowing down. The relaxation time τ_l can be described by a power-law form

$$\tau_l = \tau_l^{(0)} (T/T_l^* - 1)^{-x_l}, \tag{13}$$

where x_l is a critical exponent and T_l^* is a finite critical temperature. The least-squares fit of the data for $1.9 \leqslant T \leqslant 2.6$ K to Eq. (13) yields the parameters $T_l^* = 1.02 \pm 0.55$ K and $x_l = 22.52 \pm 10.45$. The uncertainty of x_l is too large. The value of T_l^* may be appropriate.

For $2.4 \leqslant T \leqslant 3$ K, instead of a peak, χ''_{aa} has a local minimum at a characteristic frequency that shifts to the low-frequency side with decreasing temperature [see Fig. 9(b)]. For $3.1 \leqslant T \leqslant 4.3$ K, χ''_{aa} decreases with increasing frequency [see Fig. 9(c)]. The f dependence of χ''_{aa} can be well described by a power-law form ($\chi''_{aa} \approx \omega^{-y}$) in the limited low-frequency range $0.01 \leqslant f \leqslant 20$ Hz. The exponent y also depends on temperature: the exponent y has a shoulder (≈ 0.065) around 2.9 K and a broad peak ($= 0.085$) around 4 K. The value of y is larger than that of x for the same T contrary to the prediction from the Kramers-Kronig relation that y should be the same as x. According to the fluctuation-dissipation theorem, the Fourier spectrum $S_{aa}(\omega)$ of the time-dependent magnetization fluctuation $\langle M_a(0) M_a(t) \rangle$ is related to $\chi''_{aa}(\omega)$ by

$$S_{aa}(\omega) = \int_{-\infty}^{\infty} \langle M_a(0) M_a(t) \rangle e^{-i\omega t} dt = \frac{2k_B T}{\hbar\omega} \chi''_{aa}(\omega), \tag{14}$$

where $M_a(t)$ is the time-dependent magnetization. Thus, $S_{aa}(\omega)$ has the form $\omega^{-(1+y)}$, indicating that $\langle M_a(0) M_a(t) \rangle$ varies with t as t^y.

For $4.5 \leqslant T \leqslant 6.1$ K χ''_{aa} shows a peak at a characteristic frequency f_h that increases with increasing frequency. The relation of T vs f_h thus obtained is equivalent to that of T_h vs f [see Fig. 3(d)] derived from the data of χ''_{aa} vs T with frequency as a parameter: T_h clearly increases with increasing frequency. Such behavior is common to spin-glass phases. The peak temperature T_h may correspond to the spin freezing temperature $T_{\mathrm{SG}}^{(h)}$. In Fig. 10 we show the T dependence of the average relaxation time τ_h, where τ_h is determined using the relation that the peak of χ''_{aa} vs T appears when $\omega\tau_h = 1$ is satisfied. The least-squares fit of the data of τ_h vs T for $4.5 \leqslant T \leqslant 6.1$ K to Eq. (13) with the index h instead of l yields the parameters $x_h = 23.02 \pm 4.05$ and $T_h^* = 2.22 \pm 0.52$ K. The value of x_h is unphysically large. Note that $x_h = 13.8 \pm 1.4$ for the reentrant spin-glass phase transition in stage-2 $Cu_cCo_{1-c}Cl_2$ GIC with $c = 0.8$.[25] In Fig. 11 we show a scaling plot of $\chi''_{aa}/\chi''^{\,\max}_{aa}$ as a function of $\omega\tau_h$, where $\chi''^{\,\max}_{aa}$ is the peak height of χ''_{aa} at $\omega\tau_h = 1$. We find that almost all the data fall a universal curve for $10^{-4} \leqslant \omega\tau_h \leqslant 10^5$. The part of this curve for $10^0 \leqslant \omega\tau_h \leqslant 10^4$ is well described by a scaling function defined by

$$\frac{\chi''_{aa}}{\chi''^{\,\max}_{aa}} = \frac{G(\omega\tau_h)}{G(\omega\tau_{h=1})}, \tag{15}$$

with

$$G(\omega\tau_h) = \frac{\cos(\pi a/2)/2}{\cosh[(1-a)\ln(\omega\tau_h)] + \sin(\pi a/2)}, \tag{16}$$

where $a = 0.85 \pm 0.05$. The value of $a = 0$ corresponds to the Debye equation for relaxation with a single time constant. The high value of a indicates that an extremely broad distribution of relaxation times persists throughout the whole temperature range studied.

There are several other bits of evidence for the occurrence of the spin-glass phase below $T_{\mathrm{SG}}^{(h)}$. The first is, as shown in Fig. 2, that the magnetization M_{ZFC} deviates from M_{FC} below $T_f = 14.7$ K for the a axis and $T_f = 24$ K for the c axis. This behavior is also common to spin-glass phases. Unlike typical spin glasses, the freezing temperature T_f is much larger than $T_{\mathrm{SG}}^{(h)}$. The second bit of evidence lies in the T dependence of the nonlinear susceptibility χ_2, where χ_2 is defined by $\chi_2 = -4M'(3\omega)/h^3$ in the limit of $h \to 0$ and $\omega \to 0$. $M'(3\omega)$ is a real part of the third harmonic in-phase component of the ac magnetization and h is the amplitude of the ac magnetic field with angular frequency ω. The singularity of χ_2 is used to examine the nature of long-range order. For the usual ferromagnet and antiferromagnet where the spatial magnetic symmetry changes at the transition, the sign of χ_2 changes from negative to positive at the phase transition from the high-temperature PM phase to the low-temperature ordered phase. For a spin glass where the spatial magnetic symmetry does not change at the transition, χ_2

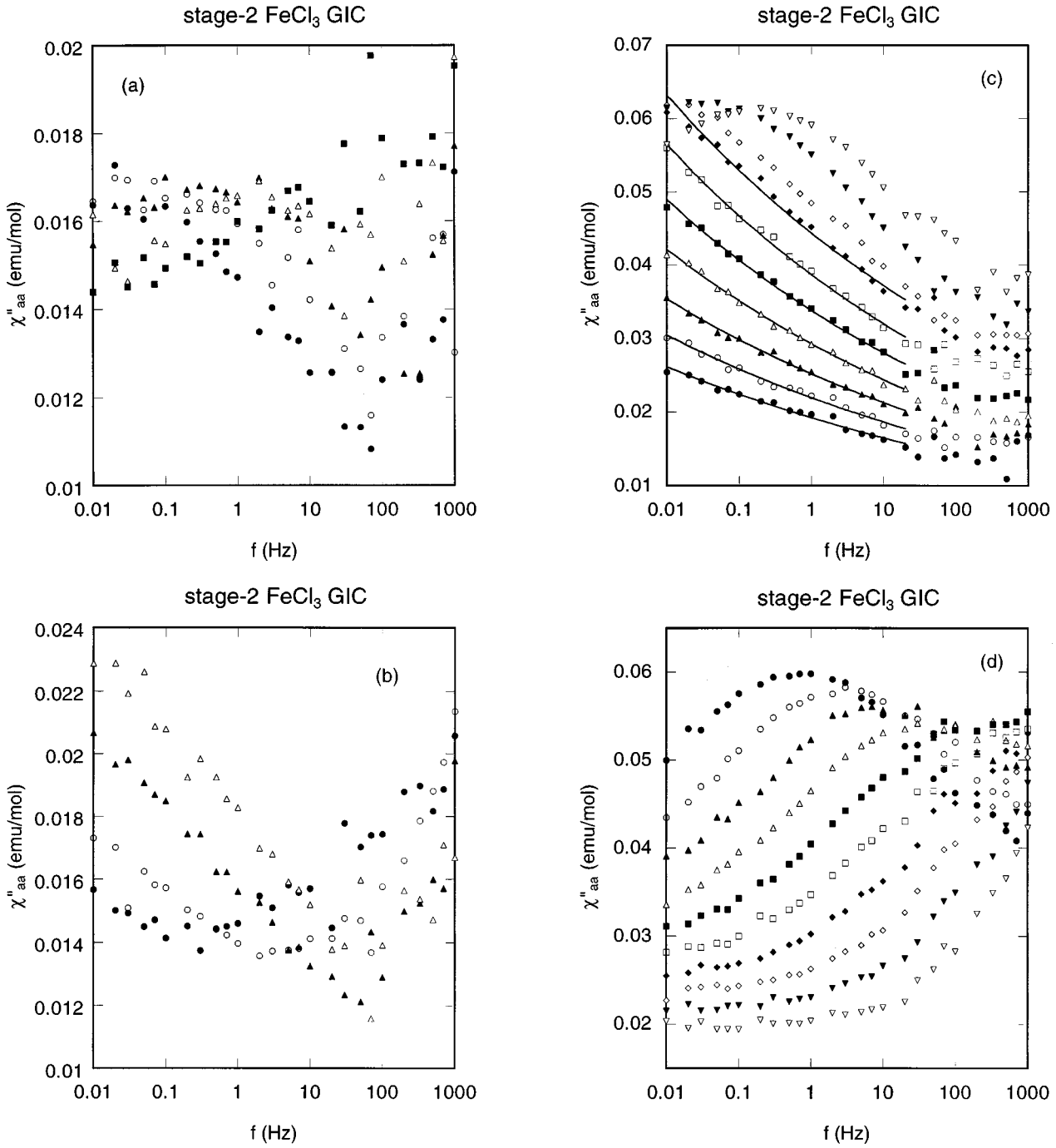

FIG. 9. f dependence of χ''_{aa} at various temperatures. $H=0$ and $h=500$ mOe. (a) $T=1.9$ (●), 2.0 (○), 2.1 (▲), 2.2 (△), and 2.3 K (■). (b) $T=2.4$ (●), 2.6 (○), 2.8 (▲), and 3.0 K (△). (c) $T=3.1$ (●), 3.3 (○), 3.5 (▲), 3.7 (△), 3.9 (■), 4.1 (□), 4.3 (♦), 4.5 (◇), 4.7 (▼), and 4.9 K (▽). The solid lines are the least-squares fits of data to the power-law form ($\chi''_{aa}\approx\omega^{-y}$) for $0.01\leqslant f\leqslant 20$ Hz. (d) $T=5.1$ (●), 5.3 (○), 5.5 (▲), 5.7 (△), 5.9 (■), 6.1 (□), 6.3 (♦), 6.5 (◇), 6.7 (▼), and 6.9 K (▽).

shows a negative divergence at the transition. Miyoshi *et al.*[9] have reported the T dependence of χ_2 for $f=3.7$, 11, 37, and 311 Hz in stage-3 $FeCl_3$ GIC. The nonlinear susceptibility χ_2 at $f=311$ Hz shows a negative peak around 7 K and changes sign around 5.5 K, while χ_2 at $f=3.7$ Hz shows a sharp peak around 6 K without the change of sign at lower temperatures. The latter result suggests that the spin-glass phase occurs at $T_{SG}^{(h)}$ without change of the spatial magnetic symmetry. Since the magnetic behavior in stage-3 $FeCl_3$ GIC is assumed to be similar to that in stage-2 $FeCl_3$ GIC, this result supports the conclusion that a spin-glass phase occurs at $T_{SG}^{(h)}$ in stage-2 $FeCl_3$ GIC. The third bit of evidence is found in the exponent α for the field dependence of the peak temperature T_h for χ'_{aa} and χ''_{aa} listed in Table I. The exponent α is rather close to that ($\alpha=1.5$) predicted by Almeida and Thouless[22] for the field dependence of freezing temperature at the transition be-

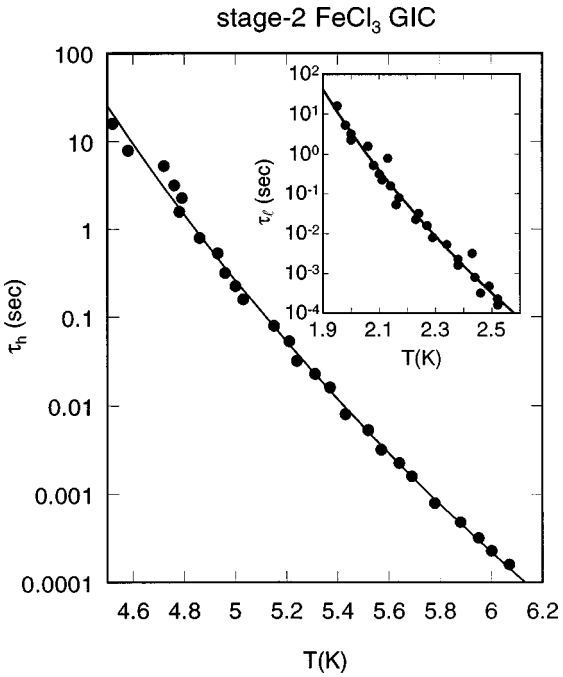

FIG. 10. T dependence of average relaxation time τ_h derived from the assumption that χ''_{aa} has a peak at $\omega\tau_h(T)=1$ for each frequency f. The inset shows the T dependence of τ_l in the low-temperature range. The solid lines are the least-squares fits of data to Eq. (13).

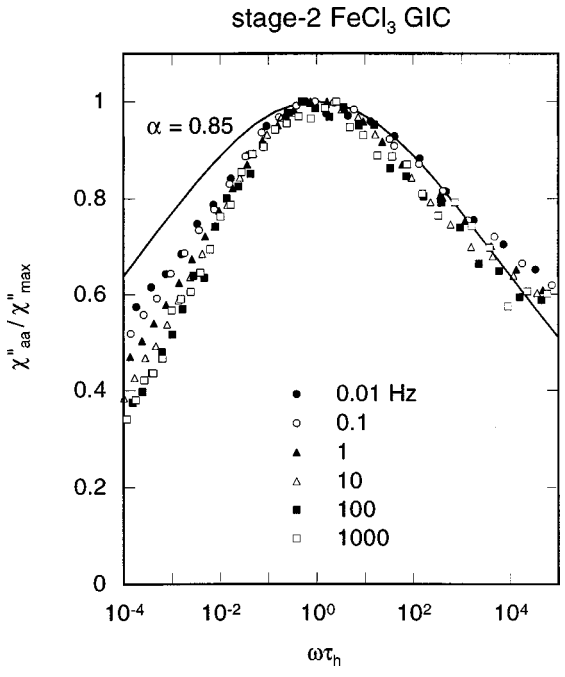

FIG. 11. Scaling plot of $\chi''_{aa}/\chi''^{\,\max}_{aa}$ as a function of $\omega\tau_h$, where $\tau_h=\tau_h^0\ (T/T^*-1)^{-x_h}$ with $\tau_h^0=44.6$ s, $x_h=23.02$, and $T_h^*=2.22$ K. The scaling function given by Eq. (15) is shown by the solid line ($a=0.85$).

tween the PM phase and the SG phase. Note that the frequency dependence of α is not sufficiently understood at present.

D. Origin of the spin-glass phase at $T_{\rm SG}^{(h)}$

We consider here the origin of the spin-glass phase at $T_{\rm SG}^{(h)}$. As described in Sec. II, the Mössbauer measurements show that there are three kinds of Fe site in the $FeCl_3$ layers: the majority Fe^{3+} (site A), the minority Fe^{2+} (site B), and the minority Fe^{3+} (site C). The percent contribution of majority Fe^{3+} is 75.6% at 10 K. The easy axis of majority Fe^{3+} spins lies in the c plane. The intraplanar exchange interaction between Fe^{3+} is antiferromagnetic: $J=-0.415\pm0.047$ K. The percent contribution of Fe^{2+} ions is 17% at 10 K as the temperature decreases. The easy axis of minority Fe^{2+} spins is along the c axis. The intraplanar exchange interaction between Fe^{2+} spins may be ferromagnetic. The magnetic behavior of Fe^{2+} spins in $FeCl_3$ GIC may be similar to those of Fe^{2+} spins in stage-2 $FeCl_2$ GIC that behaves like a 2D Ising ferromagnet on the triangular lattice. Ohhashi and Tsujikawa[17] have reported that the dc magnetic susceptibility of stage-2 $FeCl_2$ GIC obeys a Curie-Weiss law as $\Theta_c=16\pm1$ K and $\Theta_a=14\pm1$ K. Since $z=6$ is the number of nearest-neighbor Fe^{2+} ions and spin S $(=1)$ of Fe^{2+} ions is a fictitious spin, the intraplanar ferromagnetic exchange interaction between Fe^{2+} spins is estimated as $J=1.75\pm0.13$ K from Θ_a, which is stronger than the intraplanar antiferromagnetic exchange interaction J between Fe^{3+} spins. The spin-glass phase at $T_{\rm SG}^{(h)}$ may result from (i) the competition between spin anisotropy (XY for Fe^{3+} and Ising for Fe^{2+}) and (ii) the competition between intraplanar exchange interactions (antiferromagnetic for Fe^{3+} and ferromagnetic for Fe^{2+}).

The minority Fe^{3+} ions (site C) are next neighbors to iron vacancies. The percent contribution of these Fe^{3+} ions remains unchanged: 7.4% at 10 K. The number of iron vacancies is one third of the number of Fe^{3+} sites nearest neighbors to iron vacancies (2.8%). The increase in the number of vacancies is equivalent to the dilution of the system with nonmagnetic impurities. In $FeCl_3$ GIC's with a honeycomb lattice with $z=3$, the percolation threshold c_p is predicted as $c_p=0.70$. For $c<c_p$, no long-range spin order exists. Since the concentration of Fe ions may coincide with $c=0.972$, the existence of vacancies is not so significant to the spin-glass phase.

Here we discuss the T dependence of χ'_{aa}, χ'_{cc}, χ''_{aa}, and χ''_{cc}. As shown in Figs. 3(a) and 5(a), the peak height of χ'_{aa} at $T_{\rm SG}^{(h)}$ is about 40% larger than that of χ'_{cc} at the same frequency, while as shown in Figs. 3(b) and 5(b) the peak height of χ''_{aa} is about 50% larger than that of χ''_{cc}. The full width at half maximum of the peak in χ''_{cc} is narrower than that in χ''_{aa}. These results suggest that there exist competing spin anisotropies between the XY symmetry for majority Fe^{3+} spins and the Ising symmetry for the minority Fe^{2+} spins. The system still magnetically behaves like a XY antiferromagnet but the effect of Ising anisotropy on the magnetic behavior cannot be neglected. The strong divergence of the peak in χ''_{cc} is indicative of the Ising symmetry of Fe^{2+}. As shown in Fig. 3(d), the peak temperature of χ''_{aa} is higher than that of χ''_{cc}: 4.78 K for χ''_{aa} and 3.57 K for χ''_{cc} at $f=0.1$ Hz (6.07 K for χ''_{aa} and 4.74 K for χ''_{cc} at $f=1$ kHz). The peak temperature of χ'_{aa} is also higher than that of

χ'_{cc}: 5.50 K for χ'_{aa} and 4.92 K for χ'_{cc} at $f=0.1$ Hz (6.72 K for χ'_{aa} and 6.01 K for χ'_{cc} at $f=1$ kHz). When the system goes into the low-temperature phase from the paramagnetic phase, the XY components of spins are first antiferromagnetically ordered. Through an off-diagonal interaction between the spin XY component and the Ising component, the spin Ising component starts to order at a lower temperature. Similar behavior has also been observed in quasi-2D random spin systems $K_2Cu_cCo_{1-c}F_4$ (Ref. 26) where the ferromagnetic Cu^{2+} spins with XY spin anisotropy compete with the antiferromagnetic Co^{2+} spins with Ising anisotropy. For $0.50<c<0.84$ there are two kinds of SG freezing temperature, corresponding to the freezing of spin components along the c axis (at the high-temperature side) and in the c plane (at the low-temperature side), respectively.

It is known that the $FeCl_3$ layers are formed of small islands in $FeCl_3$ GIC.[27] We consider how the spin-glass phase transition at $T_{SG}^{(h)}$ is affected by the existence of small islands. The effective interplanar exchange interaction J'_{eff} is defined by $J'_{eff}=J'N(\xi_a)$ where J' is the interplanar exchange interaction and $N(\xi_a)$ is the number of spins over the in-plane spin correlation length ξ_a: $N(\xi_a)=(\pi/\sqrt{3})(\xi_a/a_h)^2$. The in-plane spin correlation length increases on approaching $T_{SG}^{(h)}$ from the high-temperature side, leading to a dramatic increase of $|J'_{eff}|$. However, the further growth of the in-plane spin correlation length is partly limited by island size, making the effective interplanar exchange interaction $|J'_{eff}|$ finite and suppressing the 3D spin ordering. Thus the existence of the spin-glass phase at $T_{SG}^{(h)}$ is energetically favorable for the system formed of small islands that has a small probability of crossover from 2D to 3D.

E. Origin of the spin-glass phase at $T_{SG}^{(l)}$

Here we discuss the origin of spin-glass phase at $T_{SG}^{(l)}$. The peak height of χ''_{aa} at $T_{SG}^{(l)}$ is much smaller than that at $T_{SG}^{(h)}$. There is no anomaly observed in χ'_{cc} and χ''_{cc}, implying that the spin component along the c axis does not contribute to the spin ordering mechanism. This spin-glass phase may result from the competition between the NN antiferromagnetic exchange interaction J_0 and the NNN ferromagnetic exchange interaction J_1. The competing spin anisotropies may not be the main cause for the spin-glass phase at $T_{SG}^{(l)}$. Similar spin-glass behavior has been reported in Ising-type dilute antiferromagnets $Fe_cMg_{1-c}Cl_2$,[28] where Fe^{2+} ions are diluted with nonmagnetic Mg^{2+} ions. The concentration $c=0.5$ corresponds to the in-plane percolation limit. For $0.5<c\leq 0.6$ the PM-AF (antiferromagnetic) transition occurs at T_N and the AF-RSG (reentrant spin glass) transition at T_{RSG} ($<T_N$). For $0.3\leq c\leq 0.5$ the PM-SG transition occurs at T_{SG}. The appearance of the SG and RSG phases at low temperatures is probably due to the competition between NN intraplanar ferromagnetic interaction and NNN intraplanar antiferromagnetic interaction.

Similar spin-glass-like behavior is also observed in stage-2 $MnCl_2$ GIC.[29–31] The dispersion χ'_{aa} shows a peak at T_c ($=1.20$ K) that shifts to the low-temperature side with decreasing frequency.[30] The absorption χ''_{aa} appears below T_c. The peak temperature T_c decreases with increasing field applied along the c plane and is well described by Eq. (2) with $\alpha=2.33\pm0.11$ and $T_c(0)=1.20$ K.[29] This value of α is relatively larger than that from the Almeida-Thouless line. The in-plane spin structure around T_c has been studied by magnetic neutron scattering.[31] The magnetic Bragg peaks appear at the in-plane wave vector $\mathbf{Q}=\mathbf{k}_1$, $\mathbf{k}_2$, $\mathbf{a}^*-\mathbf{k}_1$, $\mathbf{a}^*-\mathbf{k}_2$, and so on. Here $\mathbf{k}_1$ and $\mathbf{k}_2$ are in-plane reciprocal lattice vectors for the incommensurate magnetic modulation: $|\mathbf{k}_1|=|\mathbf{k}_2|=0.522$ Å^{-1} and $|\mathbf{a}^*|=1.965$ Å^{-1}. The angle between $\mathbf{a}^*$ and $\mathbf{k}_1$ is 30°. The ground-state in-plane spin configuration is explained by an exchange Hamiltonian that includes no fewer than three shells of nearest neighbors in the plane: small ferromagnetic NN interaction J_0, a relatively large antiferromagnetic second NN J_1, and third NN exchange interaction J_2. The spin-glass-like behavior in stage-2 $MnCl_2$ GIC may result from these competing intraplanar exchange interactions.

Here we note that our result for stage-2 $FeCl_3$ GIC is rather different from the data of a sample with the same stage that have been reported by Ibrahim and Zimmerman.[8] The dispersion χ'_{aa} shows a peak at 1.745 K at $H=0$. This peak shifts to the high-temperature side with increasing field in the low-field range. This implies that the system magnetically behaves like an XY ferromagnet. This is inconsistent with our result that the peak of χ'_{aa} shifts to the low-temperature side with increasing field, reflecting an antiferromagnetic NN exchange interaction J_0. What is the origin of this type of phase transition? Note that this peak at 1.7 K is dramatically enhanced as the number of Fe^{3+} sites that are nearest neighbors to iron vacancies is increased from 7 to 11%. This result may be explained as follows in terms of our model. The spin frustration effect results from the competing NN and NNN interactions. For a Fe^{3+} ion next to an empty Fe site the number of NN antiferromagnetic bonds decreases by one, while the number of NNN ferromagnetic couplings remains unchanged. This may imply that the contribution of ferromagnetic NNN bonds to the in-plane spin order is enhanced by an increase in the number of empty sites. The magnetic phase transition at $T_{SG}^{(l)}$ may have a ferromagnetic character as the number of empty sites increases.

VI. CONCLUSION

We have observed two kinds of spin-glass phase transition at $T_{SG}^{(h)}$ and $T_{SG}^{(l)}$ in stage-2 $FeCl_3$ GIC using SQUID ac and dc magnetic susceptibility under an experimental condition such that the measurements are made after the sample is cooled from room temperature to 1.9 K in zero magnetic field (typically 3 mOe). The $FeCl_3$ layers may be formed of majority Fe^{3+} spins with XY spin anisotropy and minority Fe^{2+} spins with Ising anisotropy. The intraplanar exchange interaction between Fe^{3+} spins is antiferromagnetic, while the intraplanar exchange interaction between Fe^{2+} spins is ferromagnetic. Both the competing spin anisotropies and competing interactions give rise to spin frustration effects, leading to spin-glass behavior around $T_{SG}^{(h)}$. The spin-glass behavior at $T_{SG}^{(h)}$ is characterized by an irreversible effect of magnetization and the frequency and field dependence of χ'_{aa}, χ'_{cc}, χ''_{aa}, and χ''_{cc}. The spin-glass transition at $T_{SG}^{(l)}$ may result from spin frustration effect arising from the com-

petition between the NN antiferromagnetic and NNN ferromagnetic intraplanar exchange interactions. Magnetic neutron-scattering studies on the in-plane spin structure below $T_{SG}^{(l)}$ are required for the further understanding of the spin-glass phase.

ACKNOWLEDGMENTS

The authors would like to thank A. W. Moore for providing them with HOPG samples. They are grateful to Charles R. Burr for a critical reading of this manuscript. This work was partly supported by NSF DMR 9625829.

[1] Yu. S. Karimov, A. V. Zvarykina, and Yu. N. Novikov, Fiz. Tverd. Tela **13**, 2836 (1971) [Sov. Phys. Solid State **13**, 2388 (1972)].
[2] K. Ohhashi and I. Tsujikawa, J. Phys. Soc. Jpn. **36**, 422 (1974).
[3] K. Ohhashi and I. Tsujikawa, J. Phys. Soc. Jpn. **36**, 980 (1974).
[4] D. Hohlwein, P. W. Readman, A. Chamberod, and J. M. Coey, Phys. Status Solidi B **64**, 305 (1974).
[5] S. E. Millman, B. W. Holmes, and G. O. Zimmerman, Solid State Commun. **43**, 903 (1982).
[6] S. E. Millman and G. O. Zimmerman, J. Phys. C **16**, L89 (1983).
[7] A. K. Ibrahim and G. O. Zimmerman, Phys. Rev. B **34**, 4224 (1986).
[8] A. K. Ibrahim and G. O. Zimmerman, Phys. Rev. B **35**, 1860 (1987).
[9] K. Miyoshi, M. Hagiwara, M. Matsuura, T. Abe, and Y. Mizutani, Physica B **237-238**, 190 (1997).
[10] G. Dresselhaus, J. T. Nicholls, and M. S. Dresselhaus, in *Graphite Intercalation Compounds II*, edited by H. Zabel and S. A. Solin (Springer-Verlag, Berlin, 1990).
[11] M. Suzuki, Crit. Rev. Solid State Mater. Sci. **16**, 237 (1990).
[12] S. E. Millman, M. R. Corson, and G. H. Hoy, Phys. Rev. B **25**, 6595 (1982).
[13] M. R. Corson, S. E. Millman, G. R. Hoy, and H. Mazurek, Solid State Commun. **42**, 667 (1982).
[14] S. E. Millman, Phys. Lett. **92A**, 441 (1982).
[15] S. E. Millman and G. Kirczenow, Solid State Commun. **44**, 1217 (1982).
[16] S. E. Millman and G. Kirczenow, Phys. Rev. B **28**, 5019 (1983).
[17] K. Ohhashi and I. Tsujikawa, J. Phys. Soc. Jpn. **37**, 63 (1974).
[18] Ch. Simon, F. Batallan, I. Rosenman, J. Schweitzer, H. Lauter, and R. Vangelisti, J. Phys. (France) Lett. **44**, L-641 (1983).
[19] I. Rosenman, F. Batallan, Ch. Simon, C. Ayache, J. Schweitzer, H. Lauter, and R. Vangelisti, Synth. Met. **12**, 439 (1985).
[20] Ch. Simon, F. Batallan, I. Rosenman, G. Furdin, R. Vangelisti, H. Lauter, J. Schweitzer, C. Ayache, and G. Pepy, Ann. Phys. (Paris) **11**, 143 (1986).
[21] Y. Mizutani, T. Abe, M. Asano, and T. Harada, J. Mater. Res. **8**, 1586 (1993).
[22] J. R. L. de Almeida and D. J. Thouless, J. Phys. A **11**, 983 (1978).
[23] K. Yosida, Prog. Theor. Phys. **6**, 691 (1951).
[24] J. P. Stampfel, W. T. Oosterhuis, B. Window, and F. de S. Barros, Phys. Rev. B **8**, 4371 (1973).
[25] I. S. Suzuki and M. Suzuki, Solid State Commun. **106**, 513 (1998).
[26] M. Itoh, I. Yamada, M. Ishizuka, K. Amaya, T. Kobayashi, K. Koga, and K. Motoya, J. Phys. Soc. Jpn. **59**, 1792 (1990).
[27] G. K. Wertheim, Solid State Commun. **38**, 633 (1981).
[28] D. Bertrand, F. Bensamka, A. R. Fert, J. Gelard, J. P. Redoules, and S. Legrand, J. Phys. C **17**, 1725 (1984).
[29] Y. Kimishima, A. Furukawa, M. Suzuki, and H. Nagano, J. Phys. C **19**, L43 (1986).
[30] M. Matsuura, Y. Karaki, T. Yonezawa, and M. Suzuki, Jpn. J. Appl. Phys., Part 1 **26**, Suppl. 26-3, 773 (1987).
[31] D. G. Wiesler, M. Suzuki, I. S. Suzuki, and N. Rosov, Phys. Rev. B **55**, 6382 (1997).